Encoding biological recognition in a bicomponent cell-membrane mimic

Cesar Rodriguez-Emmenegger[a,b], Qi Xiao[c,d], Nina Yu. Kostina[a,b], Samuel E. Sherman[c], Khosrow Rahimi[a,b], Benjamin E. Partridge[c], Shangda Li[c], Dipankar Sahoo[c], Aracelee M. Reveron Perez[c], Irene Buzzacchera[a,c,e], Hong Han[c], Meir Kerzner[c], Ishita Malhotra[c], Martin Möller[a,b], Christopher J. Wilson[e], Matthew C. Good[f,g], Mark Goulian[h,i], Tobias Baumgart[c], Michael L. Klein[d,1], and Virgil Percec[c,1]

[a]DWI–Leibniz Institute for Interactive Materials, Rheinisch-Westfälische Technische Hochschule Aachen University, 52074 Aachen, Germany; [b]Institute of Technical and Macromolecular Chemistry, Rheinisch-Westfälische Technische Hochschule Aachen University, 52074 Aachen, Germany; [c]Department of Chemistry, Roy & Diana Vagelos Laboratories, University of Pennsylvania, Philadelphia, PA 19104-6323; [d]Institute of Computational Molecular Science, Temple University, Philadelphia, PA 19122; [e]NovioSense B.V., 6534 AT Nijmegen, The Netherlands; [f]Department of Cell and Developmental Biology, Perelman School of Medicine, University of Pennsylvania, Philadelphia, PA 19104-6058; [g]Department of Bioengineering, University of Pennsylvania, Philadelphia, PA 19104-6321; [h]Department of Biology, University of Pennsylvania, PA 19104-6313; and [i]Department of Physics and Astronomy, University of Pennsylvania, Philadelphia, PA 19104-6059

Contributed by Michael L. Klein, January 22, 2019 (sent for review December 27, 2018; reviewed by Stephen Z. D. Cheng and Timothy J. Deming)

Self-assembling dendrimers have facilitated the discovery of periodic and quasiperiodic arrays of supramolecular architectures and the diverse functions derived from them. Examples are liquid quasicrystals and their approximants plus helical columns and spheres, including some that disregard chirality. The same periodic and quasiperiodic arrays were subsequently found in block copolymers, surfactants, lipids, glycolipids, and other complex molecules. Here we report the discovery of lamellar and hexagonal periodic arrays on the surface of vesicles generated from sequence-defined bicomponent monodisperse oligomers containing lipid and glycolipid mimics. These vesicles, known as glycodendrimersomes, act as cell-membrane mimics with hierarchical morphologies resembling bicomponent rafts. These nanosegregated morphologies diminish sugar–sugar interactions enabling stronger binding to sugar-binding proteins than densely packed arrangements of sugars. Importantly, this provides a mechanism to encode the reactivity of sugars via their interaction with sugar-binding proteins. The observed sugar phase-separated hierarchical arrays with lamellar and hexagonal morphologies that encode biological recognition are among the most complex architectures yet discovered in soft matter. The enhanced reactivity of the sugar displays likely has applications in material science and nanomedicine, with potential to evolve into related technologies.

Janus glycodendrimers | lipid rafts | nanosegregation | atomic force microscopy | galectin

Soft matter self-organizes into a diversity of periodic and quasiperiodic arrays, including Frank–Kasper phases such as cubic $Pm\bar{3}n$, known also as the A15 phase (1–4), tetragonal $P4_2/mnm$ known the σ-phase (5), dodecagonal liquid quasicrystals (6–8), plus helical columns (9) and spheres (10), including some that disregard chirality. The aforementioned morphologies are responsible for a variety of functions in soft matter and biology (3, 11–15). These complex architectures, which were discovered and elucidated via structural and retrostructural analysis of libraries of self-assembling dendrons and dendrimers, employed diffraction methods analogous to those used to develop the field of structural biology (16). Later these same phases were found by the same methods (17) in block copolymers (18–22), surfactants (23–26), lipids (27–33), glycolipids (34), and in other systems (35–38). Recently, amphiphilic Janus dendrimers (JDs) (39, 40), and their sugar-presenting analogs, Janus glycodendrimers (JGDs) (41), which provide synthetic alternatives to natural lipids and glycolipids that are readily functionalized, have been reported to self-assemble in either water or buffer (42) into vesicles, named dendrimersomes (DSs) and glycodendrimersomes (GDSs) (43), respectively. They can also be made into cell-like hybrids with either bacterial (44) or human cells (45). As with cell membranes, the bilayers of these supramolecular constructs act as a barrier between the inside and outside of DSs, GDSs, and cell-like hybrids (39, 40, 43, 44). Selective permeation can be provided, with comparable efficiency as with liposomes (13) and polymersomes (46), when either transmembrane proteins or their mimics are incorporated into the bilayer (44). Thus, DSs and GDSs can be used as biological-membrane mimics to elucidate concepts in cell biology and glycobiology, such as compartmentalization, encapsulation and release, selective transport (39, 40, 43, 44), as well as fusion and fission (47–49). Intriguingly, while searching for the minimum concentration of sugar from JGDs that is able to aggregate proteins, we discovered that sequence-defined monodisperse JGDs containing D-lactose (Lac) or D-mannose exhibit higher activity toward sugar-binding proteins, known as lectins, on decreasing surface density of sugar (50–52). This inverse relationship between sugar density and aggregation of lectins is opposite to what is expected

Significance

The seminal fluid mosaic model of the cell membranes suggests a lipid bilayer sea, in which cholesterol, proteins, glycoconjugates, and other components are swimming. Complementing this view, a microsegregated rafts model predicts clusters of components that function as relay stations for intracellular signaling and trafficking. However, elucidating the arrangement of glycoconjugates responsible for communication and recognition between cells, and cells with proteins remains a challenge. Herein, designed dendritic macromolecules are shown to self-assemble into vesicles that function as biological-membrane mimics with controlled density of sugar moieties on their periphery. Surprisingly, lowering sugar density elicits higher bioactivity to sugar-binding proteins. This finding informs a design principle for active complex soft matter with potential for applications in cellular biology and nanomedicine.

Author contributions: C.R.-E., Q.X., M.L.K., and V.P. designed research; C.R.-E., Q.X., N.Y.K., S.E.S., K.R., B.E.P., S.L., D.S., A.M.R.P., I.B., H.H., M.K., and I.M. performed research; M.M., C.J.W., M.C.G., M.G., and T.B. contributed new reagents/analytic tools; C.R.-E., Q.X., N.Y.K., B.E.P., M.L.K., and V.P. analyzed data; and C.R.-E., Q.X., N.Y.K., B.E.P., M.L.K., and V.P. wrote the paper.

Reviewers: S.Z.D.C., The University of Akron; and T.J.D., University of California, Los Angeles.

The authors declare no conflict of interest.

[1]To whom correspondence may be addressed. Email: mlklein@temple.edu or percec@sas.upenn.edu.

This article contains supporting information online at www.pnas.org/lookup/suppl/doi:10.1073/pnas.1821924116/-/DCSupplemental.

Published online February 28, 2019.

from classic kinetics (53, 54). Although the molecular structure of the JGDs exhibiting increased reactivity with decreasing sugar density is known (50–52), the three-dimensional structure providing this function is not understood. Indeed, elucidating the arrangement of glycoconjugates responsible for communication and recognition between cells, and cells with proteins (49, 55), remains a major challenge. Progress toward this goal, which will also enable the design of glycoconjugate-based biomaterials, is reported here.

Seminal models of the structure of the cell membrane, including the lipid bilayer sea of the fluid mosaic model (56), and the microsegregated rafts model (57, 58), recognize that there are certain structures responsible for sugar (glycan) activity but have not fully elucidated the details of these structures. This is mostly since X-ray and other diffraction methods employed in the structural and retrostructural analysis of biological system and of dendrimer assemblies cannot be easily applied to the analysis of fluid natural and synthetic cell membranes (59–61).

Here, we employ an analysis of atomic force microscopy images and their associated fast Fourier transforms (FFTs), along with complementary molecular modeling, to address the question of what architectures program enhanced glycan function of JGDs vesicles. This diffraction-like methodology reveals that a complex (62, 63) hierarchical self-organization of sugar moieties arranged into lamellar and hexagonal nanophase-separated periodic arrays are responsible for the enhanced activity compared with GDS where sugars were densely packed and do not exhibit nanomorphologies. Such dense packing presumably results in stronger sugar–sugar interactions ultimately reducing their availability for binding to galectins. Furthermore, these bicomponent patterned hierarchical nanoarchitectures may provide a general mechanism to program and encode biological recognition and function of glycan, not only on bicomponent GDSs, but also on the surface of different vesicles containing glycoconjugates such as liposomes, polymersomes, synthetic cells, hybrid cells, and other globular assemblies.

Results and Discussion

Accelerated Modular Synthesis of JGDs and Sequence-Defined Oligomeric JGDs. GDSs were self-assembled from sequence-defined JGDs (Figs. 1 and 2*A*). All JGDs in this work contain Lac, a sugar commonly found in human cells, and triethylene glycol (3EO) fragments (Figs. 1 and 2*B*) as their hydrophilic components. Lac substituents are diluted by increasing the number of 3EO substituents to create a library with systematic structural variation. The synthesis of **JGD-4$_{Lac}$** is shown in *SI Appendix*, Figs. S1–S8, while that of **JGD(5/1$_{Lac}^{2}$)** and **JGD(5/1$_{Lac}^{3}$)** in *SI Appendix*, Figs. S9–S17.

Other JGDs (Fig. 1) were prepared as previously reported by accelerated iterative modular synthesis (39, 51), similar to **JGD-4$_{Lac}$**. These JGDs share the same hydrophobic part containing 3,5-bis(dodecyloxy)benzoic esters. A library including high-sugar-density single–single **JGD-1$_{Lac}$**, twin–twin **JGD-2$_{Lac}$**, and tetra–tetra **JGD-4$_{Lac}$**, and sequence-defined JGDs with relatively low-sugar density were involved in this study. The sugar densities decreased from 100% Lac (**JGD-1$_{Lac}$**, **JGD-2$_{Lac}$**, and **JGD-4$_{Lac}$**) to 3/1 (3EO/Lac) for **JGD(3/1$_{Lac}$)**, 5/1 (for 3EO/Lac) for **JGD(5/1$_{Lac}^{2}$)** and **JGD(5/1$_{Lac}^{3}$)**, 6/1 (3EO/Lac) for **JGD(6/1$_{Lac}$)**, and 8/1 (3EO/Lac) for **JGD(8/1$_{Lac}^{2S}$)**, **JGD(8/1$_{Lac}^{3S}$)**, **JGD(8/1$_{Lac}^{2L}$)**, and **JGD(8/1$_{Lac}^{3L}$)**.

The position of Lac on the hydrophilic 3EO dendrons was tuned in the 8/1 (3EO/Lac) sequence-defined JGDs. Lac was appended in the 2 position (counted from left to right) of the gallic amide for **JGD(8/1$_{Lac}^{2S}$)** and **JGD(8/1$_{Lac}^{2L}$)**, and in the 3 position for **JGD(8/1$_{Lac}^{3S}$)** and **JGD(8/1$_{Lac}^{3L}$)**. The linker lengths of the sequence-defined JGDs were changed from a single 3EO unit (short linker, denoted as S) in **JGD(8/1$_{Lac}^{2S}$)** and **JGD(8/1$_{Lac}^{3S}$)** to two 3EO units (long linker, denoted as L) in **JGD(8/1$_{Lac}^{2L}$)** and **JGD(8/1$_{Lac}^{3L}$)**.

Hierarchical Periodic Glycan Arrays Self-Organized by Self-Assembly of High-Density and Sequence-Defined JGDs. Lectins are proteins which recognize glycoconjugates on the cell membranes and thus mediate communication between cells with cell and with proteins. GDSs self-assembled from libraries of JGDs unveiled how the structures of lectins affect their bioactivity toward recognition by investigating the cross-linking of cell-like GDSs and the functional pairing between the cognate sugars and lectins (64–68). Lac-presenting JGDs were selected for the present study since they self-assemble into unilamellar vesicles comparatively simpler than those of onion-like multilamellar vesicles self-assembled from Man-presenting JGDs and since Lac is larger than Man and which is expected to facilitate analysis by atomic force microscopy (AFM) experiments.

Aggregation of GDSs with wild-type human galectin-1 (Gal-1) (Fig. 2*C*) reproduces the unexpected but general trend of an increase in activity of GDSs with decreasing density of sugars reported previously in both unilamellar (51) and onion-like (52) GDSs. There is a modest, yet statistically significant, increase in the activity from **JGD-1$_{Lac}$** to **JGD-2$_{Lac}$**, and to **JGD-4$_{Lac}$** (Fig. 2*C* and *SI Appendix*, Fig. S18), as expected by multivalency (53, 54). There is a marked increase in aggregation activity when the sugar density is decreased, in sequence-defined **JGD(5/1$_{Lac}^{2}$)**, **JGD(6/1$_{Lac}^{3}$)**, **JGD(6/1$_{Lac}$)**, **JGD(8/1$_{Lac}^{2S}$)**, **JGD(8/1$_{Lac}^{3S}$)**, **JGD(8/1$_{Lac}^{2L}$)**, and **JGD(8/1$_{Lac}^{3L}$)** (Fig. 2*E* and *SI Appendix*, Fig. S19). Similarly, other complex galectins including heterodimeric human galectin-8S (Gal-8S) (50, 51) and engineered galectin-1 tetramer (Gal-1)$_4$–GG (67) presented trends in line with Gal-1 (Fig. 2*C*).

Structural Analysis of Lamellar Periodic Glycan Arrays of Giant GDSs Self-Organized from High-Density and Sequence-Defined JGDs. A structural analysis methodology using AFM, FFT, and molecular modeling was used to investigate the structures of GDSs (Fig. 3). Giant GDSs prepared by thin-film hydration were utilized, as the dimensions of giant GDSs (micrometer scale) rather than those of small GDSs (100–200 nm) obtained by injection (39) are required to access analysis of hierarchical nanodomains by AFM. FFT provides a diffraction-like pattern that is used for structural and retrostructural analysis. Giant GDSs prepared from **JGD-1$_{Lac}$** and **JGD-2$_{Lac}$** display a very smooth and compact surface (Fig. 4*A*) while those prepared from **JGD-4$_{Lac}$** (Fig. 4*B*), **JGD(3/1$_{Lac}$)**, **JGD(5/1$_{Lac}^{2}$)**, **JGD(6/1$_{Lac}^{3}$)**, **JGD(6/1$_{Lac}$)**, **JGD(8/1$_{Lac}^{2S}$)**, and **JGD(8/1$_{Lac}^{3S}$)** (Fig. 4*C*) unexpectedly exhibit hierarchical lamellar morphologies. Additional sequence-defined JGDs in which Lac is attached via a two-3EO linker **JGD(8/1$_{Lac}^{2L}$)**, and **JGD(8/1$_{Lac}^{3L}$)** (Fig. 2*C*) generate GDSs which exhibit hierarchical periodic arrays of glycans with hexagonal patterns (Fig. 4*D*). Although the lamellar and hexagonal periodicities of these glycan arrays resemble those of supramolecular dendrimers (11, 16) and block copolymers (18–22), the three-dimensional structures of these GDSs represent an arrangement of building blocks on the surface of a vesicle. Detailed AFM images including phase and height profiles, and additional modeling of GDSs of self-assembled JGDs, are available in *SI Appendix*, Figs. S20–S25.

What is the mechanism via which hierarchical periodic glycan arrays with programmed activity are generated and how do they influence reactivity to galectin? Homogeneous and densely packed surfaces were observed only for single–single **JGD-1$_{Lac}$** and twin–twin **JGD-2$_{Lac}$** (Figs. 1 and 2*A*) that can self-organize into GDSs with high-density bilayers (Fig. 4*A*). In contrast, tetra–tetra **JGD-4$_{Lac}$** and all sequence-defined JGDs present more complex, hierarchically self-organized nanodomain patterns (Fig. 4 *B–D*) with lamellar and hexagonal morphologies. The nanosegregation of sequence-defined JGDs may be anticipated since they are generated from dissimilar hydrophilic chemical fragments. However, the formation of nanosegregated domains by **JGD-4$_{Lac}$** is unexpected and it is presumably driven by a different mechanism than the one acting in the case of sugar dilution. Molecular modeling (Fig. 5 *A* and *B*) suggests that Lac moieties seek to maximize their interactions with each other. This can be achieved without nanosegregation in densely packed **JGD-1$_{Lac}$** and **JGD-2$_{Lac}$** (Fig. 4*B*). In contrast, the sugar moieties of **JGD-4$_{Lac}$** must cluster

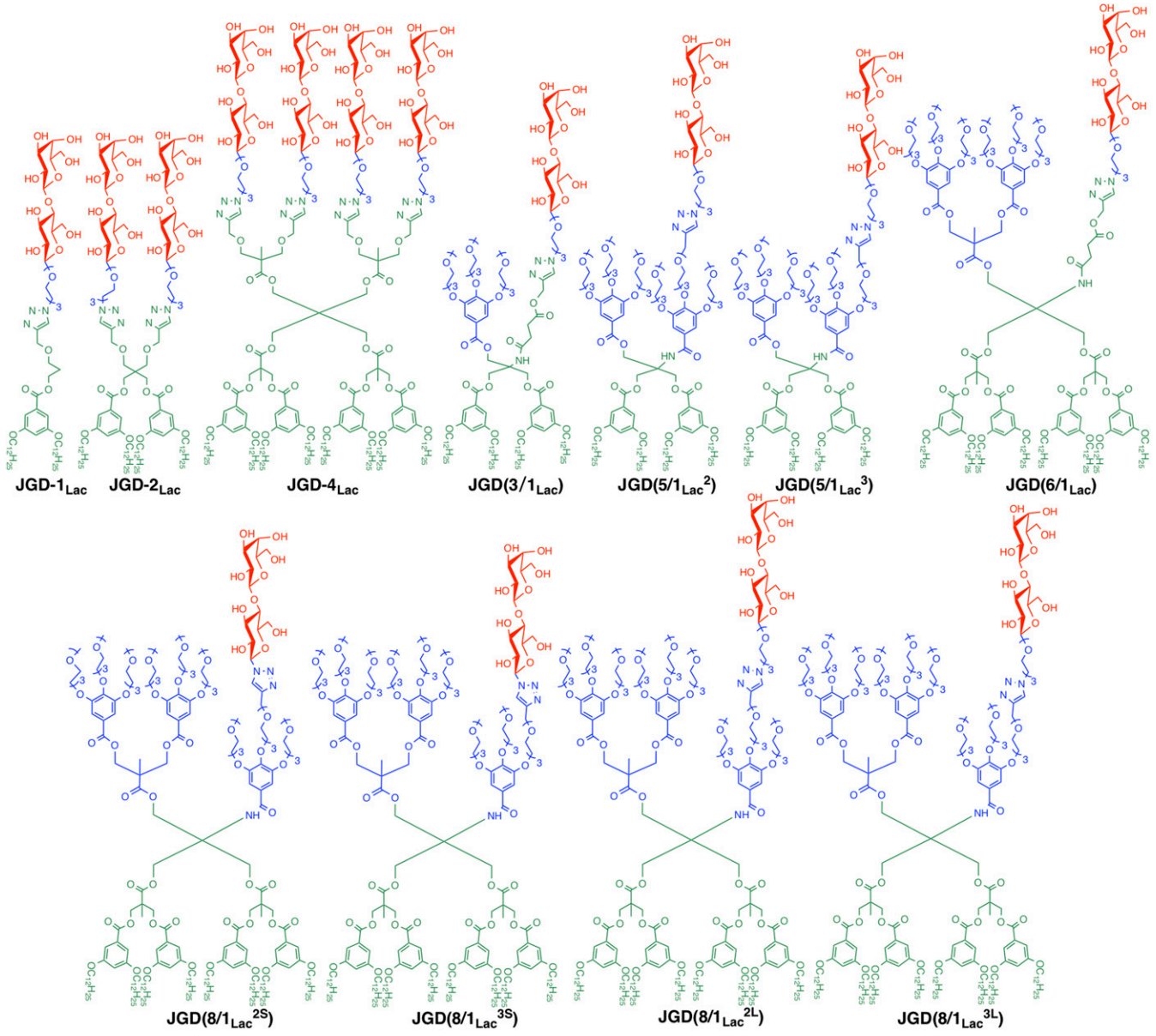

Fig. 1. Molecular structures of JGDs. Structures and short nomenclatures are shown for (*Top*) high-sugar density **JGD-1$_{Lac}$**, **JGD-2$_{Lac}$**, and **JGD-4$_{Lac}$**, and sequence-defined **JGD(3/1$_{Lac}$)**, **JGD(5/1$_{Lac}^{2}$)**, **JGD(5/1$_{Lac}^{3}$)**, **JGD(6/1$_{Lac}$)**; (*Bottom*) **JGD(8/1$_{Lac}^{2S}$)**, **JGD(8/1$_{Lac}^{3S}$)**, **JGD(8/1$_{Lac}^{2L}$)**, and **JGD(8/1$_{Lac}^{3L}$)**.

together to maximize interactions, resulting in alternating high- and low-density regions of Lac that exhibit a lamellar periodic array (Figs. 4*B* and 5 *A* and *B*). The change from **JGD-1$_{Lac}$** and **JGD-2$_{Lac}$** to **JGD-4$_{Lac}$** resembles the classic polymer effect that provides a transition from rigid to flexible backbone conformation (3).

Sequence-defined **JGD(5/1$_{Lac}^{2}$)**, **JGD(5/1$_{Lac}^{3}$)**, **JGD(6/1$_{Lac}$)**, **JGD(8/1$_{Lac}^{2S}$)**, and **JGD(8/1$_{Lac}^{3S}$)** with programmed enhanced activity generate similar periodic lamellar structures to **JGD-4$_{Lac}$**, except that both the sugar density and the steric interactions are lower than in **JGD-4$_{Lac}$** (Fig. 4 *B* and *C* and *SI Appendix*, Fig. S23). Consequently, the clusters of sugars on the surface of the GDSs self-assembled from sequence-defined JGDs are more accessible to lectin and their aggregation is therefore more efficient than for **JGD-4$_{Lac}$** even though having the same lamellar morphology (Fig. 2*C*).

Structural Analysis of Hexagonal Periodic Glycan Arrays of Giant GDSs Self-Organized from Sequence-Defined JGDs. In contrast, **JGD(8/1$_{Lac}^{2L}$)** and **JGD(8/1$_{Lac}^{3L}$)** exhibit periodic hexagonal arrays (Fig. 4*D*), as demonstrated by indexing the FFT of their AFM phase images (shown for **JGD(8/1$_{Lac}^{3L}$)** in Fig. 5*C*). This hexagonal periodic array provides an alternative morphology to enhance sugar activity. AFM height analysis (Fig. 5*D*, *Right*) shows that the isolated domains are thinner (darker in Fig. 5*D*) compared with the continuous domain (lighter in Fig. 5*D*). This suggests that the Lac moieties form the continuous domain.

A model of hexagonal nanosegregation consistent with analysis of the FFT of AFM images (Fig. 5 *E* and *F*) comprises 19 molecules of **JGD(8/1$_{Lac}^{3L}$)**: Lac moieties [red, space-filling Corey–Pauling–Koltun (CPK) view] interact at the edge of the domain, while the hydrophilic (blue) and hydrophobic (green) components of **JGD(8/1$_{Lac}^{3L}$)** occupy the remainder of the domain in three concentric layers: an outer layer (orange circles, I); an inner layer (purple circles, II); and a molecule at the center of the column (yellow circle, III). The hydrophilic and hydrophobic components of one molecule from each concentric layer are depicted in CPK view, while those of the other molecules are

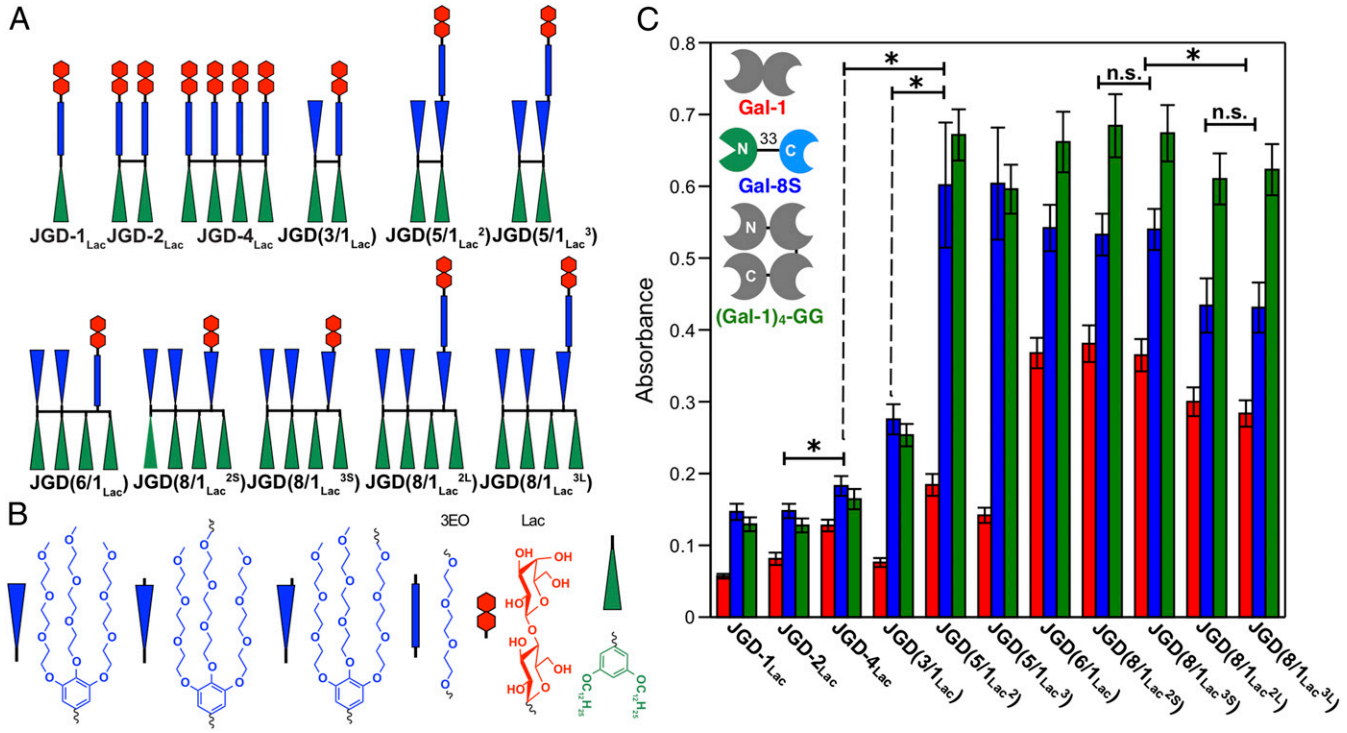

Fig. 2. Molecular architecture JGDs containing defined glycan sequence and density. (*A*) Sequence-defined JGDs with different Lac density, sequence, and linker length. (*B*) Schematic representation of JGD building blocks. (*C*) Summary of aggregation assay data using GDSs from self-assembly of sequence-defined JGDs (Lac = 0.1 mM, 900 μL) with Gal-1 (1 mg·mL^{-1}, 100 μL), Gal-8S (1 mg·mL^{-1}, 100 μL), and (Gal-1)$_4$–GG (1 mg·mL^{-1}, 100 μL). Color codes for galectins: Gal-1, red; Gal-8S, blue; (Gal-1)$_4$–GG, green. N and C represent the N and C termini of proteins. For selected examples symbols used for significant difference (*P* values by Student's *t* test) are: "n.s." for $P > 0.05$ (for statistically nonsignificant) and "*" for $P < 0.05$ (for statistically significant).

shown as faint line models for clarity. The linker of **JGD(8/1$_{Lac}^{3L}$)** molecules contains two 3EO units (Figs. 1 and 2). In molecules forming the outer layer (I), this linker is disordered beneath Lac. For molecules in the inner layer (II), the linker is more extended to allow the Lac moiety to interact with sugars from molecules in the outer layer (I). Finally, the linker of the central molecule of **JGD(8/1$_{Lac}^{3L}$)** (III) is completely extended to allow interaction between sugars. A molecule at the center of a larger domain would be unable to position its Lac moiety to allow for interaction with Lac moieties from the outer (I) and inner (II) layers, and hence the linker may restrict the size of the periodic hexagonal array. Conversely, the length of the two-3EO linker may be too long to allow sufficient confinement in periodic lamellar domains, consistent with the observation of lamellar phases only for sequence-defined JGDs with shorter single-3EO linkers, **JGD(3/1$_{Lac}$)**, **JGD(6/1$_{Lac}$)**, **JGD(8/1$_{Lac}^{2S}$)**, and **JGD(8/1$_{Lac}^{3S}$)** (Fig. 4*D* and *SI Appendix*, Fig. S24*A*). On the other hand, two sequence-defined JGDs **JGD(5/1$_{Lac}^{2}$)** and **JGD(5/1$_{Lac}^{3}$)** with two-3EO display only lamellar domains due to higher sugar density compared with **JGD(8/1$_{Lac}^{3L}$)**. These data, along with the generation of a hexagonal periodic array by a second molecule with a two-3EO linker, **JGD(8/1$_{Lac}^{2L}$)** (*SI Appendix*, Fig. S24*B*), suggest that both the linker length and sugar density determine the observed morphology. A columnar section of the bilayer comprising the repeating unit of the periodic hexagonal array (Fig. 5*F*) illustrates how hierarchical assembly of **JGD(8/1$_{Lac}^{3L}$)** (Fig. 2*A*) containing a nonaggregating single Lac becomes a very efficient ligand for aggregation with lectins. Both the hexagonal and the nondense lamellar arrays from Figs. 4 and 5 indicate potential mechanisms, which by steric constrain–release combined with self-organization (Fig. 4*B*) and/or only self-organization (Figs. 4 *C* and *D* and 5*F*), generate more reactive glycan ligands than those obtained from highly packed assemblies (Fig. 4*A*). The clustering of sugars by self-organization into lamellar and hexagonal periodic arrays reported here suggests a mechanistic explanation for the enhanced reactivity observed with sequence-defined JGDs that was not predicted by the rafts model (57, 58).

Encoding Biological Recognition by Hierarchical Nanomorphology. The goal of this paper was to report the discovery of nanoperiodic arrays on vesicles generated from sequence-defined bicomponent monodisperse oligomers containing lipid and glycolipid mimics and illustrate how they encode biological recognition and reactivity. Remarkably these nanosegregated morphologies with diminished sugar–sugar aggregation allowed the sugar to more readily bind to galectins than the densely packed arrangements of sugars, regardless of sugar dilution. The activity of these nanosegregated glycans depends on both morphology and sugar density (Fig. 2*C*). For lamellar morphology the binding to galectins increased with the decreasing density of sugar until a 1:6 dilution after which no further significant increase was observed (Fig. 2*C* and *SI Appendix*, Table S1). No statistically significant differences were observed for the binding between **JGD(8/1$_{Lac}^{2S}$)** and **JGD(8/1$_{Lac}^{3S}$)** displaying lamellar or between **JGD(8/1$_{Lac}^{2L}$)** and **JGD(8/1$_{Lac}^{3L}$)** displaying hexagonal morphology. However, a comparison between these two morphologies at the same dilution, with statistically significant results, evidenced higher activity for the lamellar, **JGD(8/1$_{Lac}^{2S}$)** and **JGD(8/1$_{Lac}^{3S}$)**, rather than for the hexagonal, **JGD(8/1$_{Lac}^{2L}$)** and **JGD(8/1$_{Lac}^{3L}$)**, organization (Fig. 2*C* and *SI Appendix*, Table S1) with Gal-1 and Gal-8S.

Conclusions

The structures, morphologies, and mechanisms via which the bicomponent sequence-defined GDSs with decreasing sugar concentration provide enhanced glycan activity have been elucidated with a diffraction-like analysis methodology. The cell-membrane

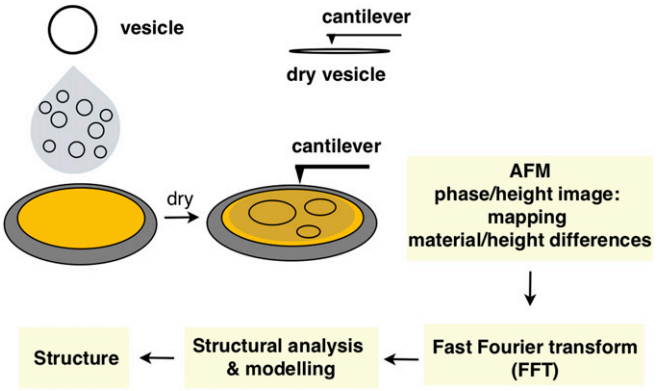

Fig. 3. Illustration of combined AFM, FFT, and modeling methodology for structural analysis.

mimic, GDSs assembled from **JGD-1$_{Lac}$** and **JGD-2$_{Lac}$** (Fig. 2*A*), display a very compact arrangement of Lac units on their surface (Fig. 4*A*). GDSs programmed to exhibit higher activity by self-assembly of sequence-defined JGDs (Figs. 2*A* and 4 *B*–*D*) self-organize hierarchical periodic arrays of glycans that reduce the dense packing of Lac. Favorable interactions with sugar-binding proteins are generated by these morphologies, resulting in an increased rate constant for aggregation, which overcomes the decrease in the concentration of the sugar on the GDS surface. This finding seemingly contradicts classic kinetic principles (53, 54), but is consistent with previous studies of self-assembled monolayers of sugars on gold surfaces (69), which demonstrated that lower sugar density provides higher affinity when applied as biosensors for lectins and viruses. However, in those studies (69), the arrangement of sugars within the monolayer was not elucidated. The hierarchical segregation of JGDs that have identical hydrophobic segments differ only in their hydrophilic parts for the self-assembly of vesicles. Neither the fluid mosaic model of the structure of cell membranes (56) nor the rafts membrane-organizing principles (57, 58) predict these glycan nanodomain morphologies on the structure of biological cell membranes or even on the structure of biological-membrane mimics. The observed hierarchical nanodomains represent an example of bicomponent rafts-like morphology that extends from a small rafts domain to the entire biological-membrane mimic and therefore could be elucidated at the molecular level. The hierarchical morphologies reported here are general for all unilamellar GDS generated by hydration and injection (41) regardless of the size of the carbohydrate from JGD and also for multilamellar "onion-like" (52) GDS. Quantitative correlations between hierarchical morphology and sugar reactivity requires the development of methodologies accessible below the limit of the diffraction of light. At the same time, these patterned nanoarchitectures are among the most complex structures yet discovered either on a planar or nonplanar surface (70–72). They provide a powerful example in which structure determines function (3, 10–14, 73), in this particular example how different supramolecular assemblies encode biological recognition. This supramolecular patterning offers a fundamental mechanism for programming enhanced activity via the surface morphology of globular glycoconjugate assemblies, such as liposomes, polymersomes, and cell-like hybrids (44, 45). Indeed, this approach informs a general design and structural analysis principle for active complex soft matter (62, 63), which will enable technological applications ranging from materials science to nanomedicine (74). It remains to be seen if bottom-up approaches derived from FFT of AFM (75) images elaborated here can overcome the limits of other methods employed in the analysis of rafts (59–61, 76, 77).

Methods

Preparation of Nanoscale GDSs by Injection. A stock solution was prepared by dissolving the required amount of amphiphilic JGDs in THF. GDSs were then generated by injection of 50 μL of the stock solution into 1.0 mL PBS, followed by 5-s vortexing.

Preparation of Giant GDSs by Hydration. A solution of JGDs in THF (100 μL) was deposited on the top surface of a roughened Teflon sheet (1 cm^2), placed in a flat-bottom vial, followed by evaporation of the solvent for 2 h. The Teflon sheet was dried in vacuo for an additional 12 h. Milli-Q water (1.0 mL) was added to submerge the film on the Teflon sheet, and the vial was placed in a 60 °C oven for 12 h for hydration. The sample was then mixed using a vortex mixer for 30 s with a final concentration of 1 mg·mL^{-1}.

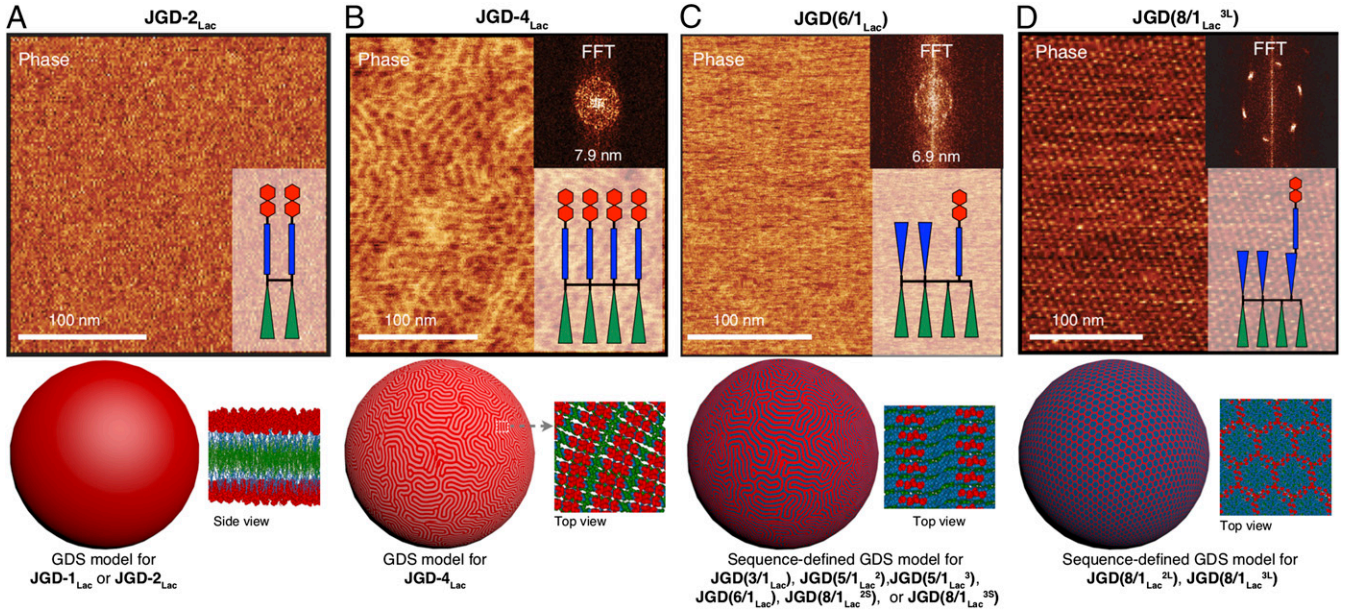

Fig. 4. Surface topology of GDS formed by self-organization of JGDs depends on glycan sequence and density. (*A*) **JGD-2$_{Lac}$**; (*B*) **JGD-4$_{Lac}$**; (*C*) **JGD(6/1$_{Lac}$)**; (*D*) **JGD(8/1$_{Lac}^{3L}$)**. (*B*–*D*, *Inset*) FFT of AFM phase images. Color code: red, sugars; blue, hydrophilic 3EO; green, hydrophobic alkyl.

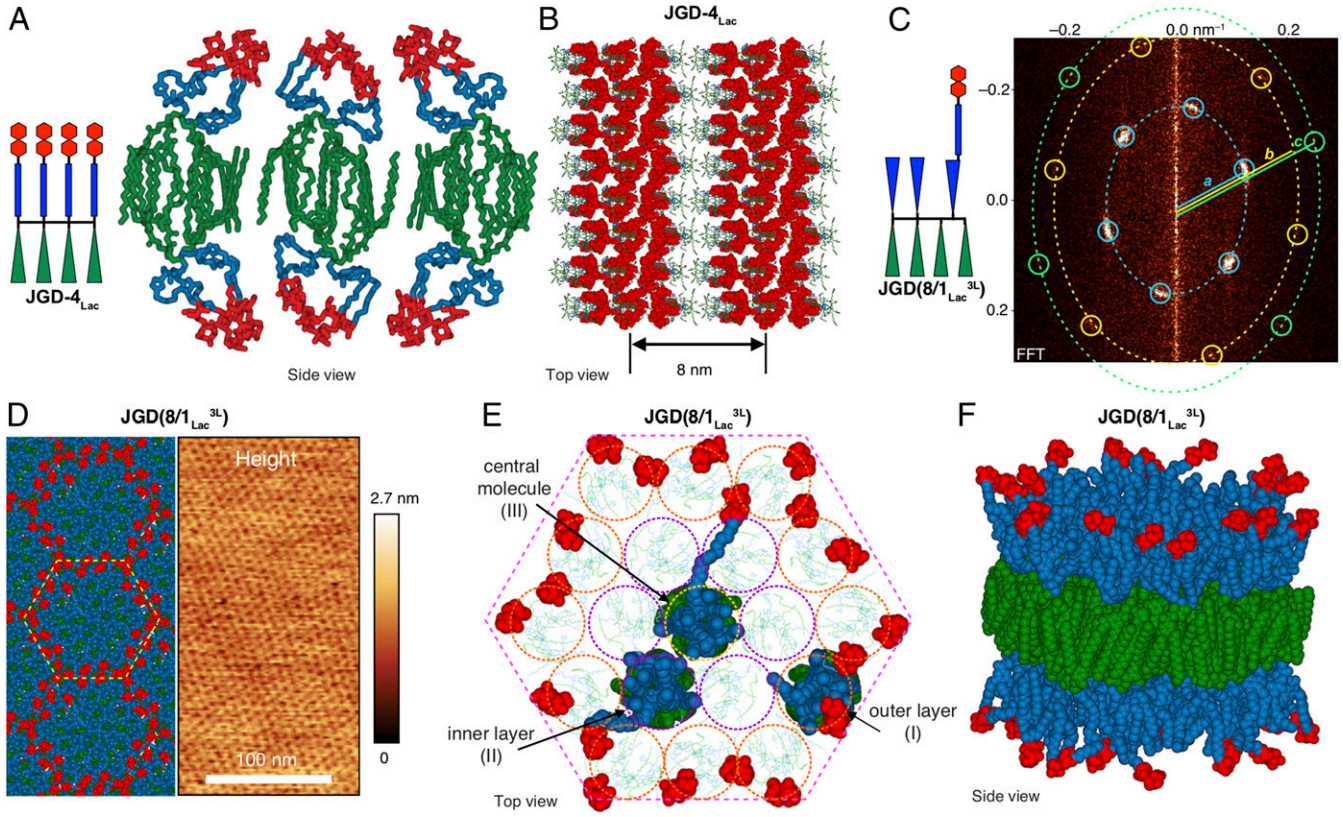

Fig. 5. Models of nanosegregated bilayer structures. (*A* and *B*) Models of **JGD-4$_{Lac}$**: (*A*) single sugar cluster comprising three molecules on each side of the bilayer; (*B*) sugar clusters in bilayer. (*C*) FFT of the AFM phase image of **JGD(8/1$_{Lac}^{3L}$)** (Fig. 4*D*) shows multiple features consistent with formation of a hexagonal array. Blue, yellow, and green circles indicate (10), (11), and (20) features, respectively. The theoretical ratio *a*:*b*:*c* for a hexagonal array is 1:$\sqrt{3}$ (=1.73):2; the observed ratio *a*:*b*:*c* is 1:1.75:2.04. (*D*, *Left*) Model of hexagonal nanosegregation and (*D*, *Right*) AFM height image of **JGD(8/1$_{Lac}^{3L}$)**. (*E*) Top view of bilayer model with all Lac moieties and three highlighted **JGD(8/1$_{Lac}^{3L}$)** molecules in CPK view. (*F*) Side view of a column of the bilayer of **JGD(8/1$_{Lac}^{3L}$)**.

AFM. The GDSs in water (~0.3 mg·mL^{-1}) were deposited and slowly dried on the freshly peeled mica. All images were acquired with a Multimode AFM NanoScope V (Digital Instruments) as topological scans in tapping mode in air, using silicon probes OTESPA-R3 (Bruker) with a nominal spring constant of 26 N·m^{-1} and a tip radius of 7 nm. The phase images were obtained by monitoring the phase lag of the cantilever vibration compared with the *z*-piezo-drive voltage while the probe scans the surface with a preset constant amplitude of vibration. The phase data contain additional information about the tip–sample interactions resulting from adhesion, surface stiffness, and viscoelastic effects. The AFM scans including FFT were analyzed using Gwyddion software.

Cryogenic Transmission Electron Microscopy. Cryogenic transmission electron microscopy (cryo-TEM) micrographs were taken on a Carl Zeiss Libra 120 microscope. Cryo-TEM samples were prepared by plunge freezing of aqueous dispersion on plasma-treated lacey grids. The vitrified specimens were transferred to a Gatan-910 cryoholder. The images were recorded at a temperature of −170 °C with an acceleration voltage of 120 kV. The GDS vesicle structures of **JGD-1$_{Lac}$**, **JGD-2$_{Lac}$**, **JGD(3/1$_{Lac}$)**, **JGD(6/1$_{Lac}$)**, **JGD(8/1$_{Lac}^{2S}$)**, **JGD(8/1$_{Lac}^{3S}$)**, **JGD(8/1$_{Lac}^{2L}$)**, and **JGD(8/1$_{Lac}^{3L}$)** were synthesized and characterized as reported previously (51, 65). Additional cryo-TEM images are presented in *SI Appendix*, Fig. S26.

Modeling of Bilayers and Vesicles. Models of bilayers in Figs. 4 and 5 and *SI Appendix*, Fig. S25 are idealized depictions of the arrangement of JDs and GSDs within a vesicle, consistent with height and phase profiles obtained by AFM. The energy of molecular structures was minimized using Chem3D (MM2 module), and then the torsional angles of bonds at the core of the dendrimer were modified in Accelrys Discovery Studio to provide segregation between the hydrophilic and hydrophobic portions of the molecule. Assemblies were generated by manual placement of molecules in Accelrys DS ViewerPro 5.0. The height profile of the assembly model was calculated and compared against experimental data obtained from AFM. The model was iteratively refined until good agreement between calculated height profile and experimental height or phase profile was obtained.

Models of vesicles in Fig. 4 are schematic depictions of the general topology of the surface of the GDS vesicle and are not to scale. These models were prepared using Autodesk 3DS Max 2017.

Aggregation Assays. Aggregation assays of GDSs with lectins were monitored in semimicrodisposable cuvettes (path length, l = 0.23 cm) at 23 °C at wavelength λ = 450 nm by using a Shimadzu UV-*vis* spectrophotometer UV-1601 with Shimadzu/UV Probe software in kinetic mode. PBS solution of galectin (100 μL) was injected into PBS solution of GDSs (900 μL). The cuvette was shaken by hand for 1–2 s before data collection was started. The same solution of GDSs solution was used as a reference. PBS solutions of galectin were prepared before the agglutination assays and were maintained at 0 °C (ice bath) before data collection.

ACKNOWLEDGMENTS. The authors thank Professor Hans-Joachim Gabius of Ludwig Maximilian University, Munich for providing lectin samples and for discussions; Dr. Mihai Peterca for discussions; and the two reviewers for constructive suggestions and recommendations. This work was supported by National Science Foundation Grants DMR-1066116 and DMR-1807127 (to V.P.); the P. Roy Vagelos Chair at the University of Pennsylvania (V.P.); the Alexander von Humboldt Foundation (N.Y.K. and V.P.); National Science Foundation Grants DMR-1120901 (to M.L.K., M.G., and V.P.) and DMR-1720530 (to M.G. and V.P.); National Institutes of Health Grant R01-GM080279 (to M.G.); Howard Hughes Medical Institute for an International Student Research Fellowship (to B.E.P.); the European Union's Horizon 2020 research and innovation programme under the Marie Skłodowska-Curie Grant Agreement 642687 (to I.B.); and financial support from Nankai University (H.H.).

1. Balagurusamy VSK, Ungar G, Percec V, Johansson G (1997) Rational design of the first spherical supramolecular dendrimers self-organized in a novel thermotropic cubic liquid-crystalline phase and the determination of their shape by X-ray analysis. *J Am Chem Soc* 119:1539–1555.
2. Hudson SD, et al. (1997) Direct visualization of individual cylindrical and spherical supramolecular dendrimers. *Science* 278:449–452.
3. Percec V, et al. (1998) Controlling polymer shape through the self-assembly of dendritic side-groups. *Nature* 391:161–164.
4. Dukeson DR, et al. (2003) Application of isomorphous replacement in the structure determination of a cubic liquid crystal phase and location of counterions. *J Am Chem Soc* 125:15974–15980.
5. Ungar G, Liu Y, Zeng X, Percec V, Cho W-D (2003) Giant supramolecular liquid crystal lattice. *Science* 299:1208–1211.
6. Zeng X, et al. (2004) Supramolecular dendritic liquid quasicrystals. *Nature* 428:157–160.
7. Ungar G, Percec V, Zeng X, Leowanawat P (2011) Liquid quasicrystals. *Isr J Chem* 51:1206–1215.
8. Holerca MN, et al. (2018) Dendronized poly(2-oxazoline) displays within only five monomer repeat units liquid quasicrystal, A15 and σ Frank–Kasper phases. *J Am Chem Soc* 140:16941–16947.
9. Roche C, et al. (2014) Homochiral columns constructed by chiral self-sorting during supramolecular helical organization of hat-shaped molecules. *J Am Chem Soc* 136:7169–7185.
10. Percec V, et al. (2009) Self-assembly of dendronized triphenylenes into helical pyramidal columns and chiral spheres. *J Am Chem Soc* 131:7662–7677.
11. Sun H-J, Zhang S, Percec V (2015) From structure to function via complex supramolecular dendrimer systems. *Chem Soc Rev* 44:3900–3923.
12. Percec V, et al. (2002) Self-organization of supramolecular helical dendrimers into complex electronic materials. *Nature* 419:384–387.
13. Percec V, et al. (2004) Self-assembly of amphiphilic dendritic dipeptides into helical pores. *Nature* 430:764–768.
14. Percec V, Rudick JG, Peterca M, Heiney PA (2008) Nanomechanical function from self-organizable dendronized helical polyphenylacetylenes. *J Am Chem Soc* 130:7503–7508.
15. Feringa BL, Browne WR (2008) Nanomechanics: Macromolecules flex their muscles. *Nat Nanotechnol* 3:383–384.
16. Rosen BM, et al. (2009) Dendron-mediated self-assembly, disassembly, and self-organization of complex systems. *Chem Rev* 109:6275–6540.
17. Peterca M, Percec V (2010) Materials science. Recasting metal alloy phases with block copolymers. *Science* 330:333–334.
18. Lee S, Bluemle MJ, Bates FS (2010) Discovery of a Frank-Kasper σ phase in sphere-forming block copolymer melts. *Science* 330:349–353.
19. Bates FS, et al. (2012) Multiblock polymers: Panacea or Pandora's box? *Science* 336:434–440.
20. Gillard TM, Lee S, Bates FS (2016) Dodecagonal quasicrystalline order in a diblock copolymer melt. *Proc Natl Acad Sci USA* 113:5167–5172.
21. Chanpuriya S, et al. (2016) Cornucopia of nanoscale ordered phases in sphere-forming tetrablock terpolymers. *ACS Nano* 10:4961–4972.
22. Kim K, et al. (2017) Thermal processing of diblock copolymer melts mimics metallurgy. *Science* 356:520–523.
23. Perroni DV, Mahanthappa MK (2013) Inverse Pm3n cubic micellar lyotropic phases from zwitterionic triazolium gemini surfactants. *Soft Matter* 9:7919–7922.
24. Yue K, et al. (2016) Geometry induced sequence of nanoscale Frank-Kasper and quasicrystal mesophases in giant surfactants. *Proc Natl Acad Sci USA* 113:14195–14200.
25. Kim SA, Jeong K-J, Yethiraj A, Mahanthappa MK (2017) Low-symmetry sphere packings of simple surfactant micelles induced by ionic sphericity. *Proc Natl Acad Sci USA* 114:4072–4077.
26. Baez-Cotto CM, Mahanthappa MK (2018) Micellar mimicry of intermetallic C14 and C15 Laves phases by aqueous lyotropic self-assembly. *ACS Nano* 12:3226–3234.
27. Mariani P, Luzzati V, Delacroix H (1988) Cubic phases of lipid-containing systems. Structure analysis and biological implications. *J Mol Biol* 204:165–189.
28. Vargas R, Mariani P, Gulik A, Luzzati V (1992) Cubic phases of lipid-containing systems. The structure of phase Q223 (space group Pm3n). An X-ray scattering study. *J Mol Biol* 225:137–145.
29. Sakya P, Seddon JM, Templer RH, Mirkin RJ, Tiddy GJT (1997) Micellar cubic phases and their structural relationships: The nonionic surfactant system C12EO12/water. *Langmuir* 13:3706–3714.
30. Charvolin J, Sadoc JF (1988) Periodic systems of frustrated fluid films and "micellar" cubic structures in liquid crystals. *J Phys* 49:521–526.
31. Paccamiccio L, et al. (2006) Pressure effects on lipidic direct phases: The dodecyl trimethyl ammonium chloride-water system. *J Phys Chem B* 110:12410–12418.
32. Bastos M, et al. (2011) Lactoferrin-derived antimicrobial peptide induces a micellar cubic phase in a model membrane system. *Biophys J* 101:L20–L22.
33. Silva T, et al. (2013) Structural diversity and mode of action on lipid membranes of three lactoferrin candidacidal peptides. *Biochim Biophys Acta* 1828:1329–1339.
34. Gulik A, Delacroix H, Kirschner G, Luzzati V (1995) Polymorphism of ganglioside-water systems: A new class of micellar cubic phases. Freeze-fracture electron microscopy and X-ray scattering studies. *J Phys II* 5:445–464.
35. Huang M, et al. (2015) Self-assembly. Selective assemblies of giant tetrahedra via precisely controlled positional interactions. *Science* 348:424–428.
36. Zhang W, et al. (2016) Toward controlled hierarchical heterogeneities in giant molecules with precisely arranged nano building blocks. *ACS Cent Sci* 2:48–54.
37. Zhang W, et al. (2017) Sequence-mandated, distinct assembly of giant molecules. *Angew Chem Int Ed Engl* 56:15014–15019.
38. Ye X, et al. (2017) Quasicrystalline nanocrystal superlattice with partial matching rules. *Nat Mater* 16:214–219.
39. Percec V, et al. (2010) Self-assembly of Janus dendrimers into uniform dendrimersomes and other complex architectures. *Science* 328:1009–1014.
40. Peterca M, Percec V, Leowanawat P, Bertin A (2011) Predicting the size and properties of dendrimersomes from the lamellar structure of their amphiphilic Janus dendrimers. *J Am Chem Soc* 133:20507–20520.
41. Percec V, et al. (2013) Modular synthesis of amphiphilic Janus glycodendrimers and their self-assembly into glycodendrimersomes and other complex architectures with bioactivity to biomedically relevant lectins. *J Am Chem Soc* 135:9055–9077.
42. Ball P (2008) Water as an active constituent in cell biology. *Chem Rev* 108:74–108.
43. Sherman SE, Xiao Q, Percec V (2017) Mimicking complex biological membranes and their programmable glycan ligands with dendrimersomes and glycodendrimersomes. *Chem Rev* 117:6538–6631.
44. Xiao Q, et al. (2016) Bioactive cell-like hybrids coassembled from (glyco)dendrimersomes with bacterial membranes. *Proc Natl Acad Sci USA* 113:E1134–E1141.
45. Yadavalli SS, et al. (2019) Bioactive cell-like hybrids from dendrimersomes with a human cell membrane and its components. *Proc Natl Acad Sci USA* 116:744–752.
46. Kaucher MS, et al. (2007) Selective transport of water mediated by porous dendritic dipeptides. *J Am Chem Soc* 129:11698–11699.
47. Xiao Q, et al. (2016) Self-sorting and coassembly of fluorinated, hydrogenated, and hybrid Janus dendrimers into dendrimersomes. *J Am Chem Soc* 138:12655–12663.
48. Xiao Q, et al. (2017) Janus dendrimersomes coassembled from fluorinated, hydrogenated, and hybrid Janus dendrimers as models for cell fusion and fission. *Proc Natl Acad Sci USA* 114:E7045–E7053.
49. Bertozzi CR, Kiessling LL (2001) Chemical glycobiology. *Science* 291:2357–2364.
50. Zhang S, et al. (2015) Dissecting molecular aspects of cell interactions using glycodendrimersomes with programmable glycan presentation and engineered human lectins. *Angew Chem Int Ed Engl* 54:4036–4040.
51. Zhang S, et al. (2015) Glycodendrimersomes from sequence-defined Janus glycodendrimers reveal high activity and sensor capacity for the agglutination by natural variants of human lectins. *J Am Chem Soc* 137:13334–13344.
52. Xiao Q, et al. (2016) Onion-like glycodendrimersomes from sequence-defined Janus glycodendrimers and influence of architecture on reactivity to a lectin. *Proc Natl Acad Sci USA* 113:1162–1167.
53. Fasting C, et al. (2012) Multivalency as a chemical organization and action principle. *Angew Chem Int Ed Engl* 51:10472–10498.
54. Munoz EM, Correa J, Riguera R, Fernandez-Megia E (2013) Real-time evaluation of binding mechanisms in multivalent interactions: A surface plasmon resonance kinetic approach. *J Am Chem Soc* 135:5966–5969.
55. Seeberger PH, Werz DB (2007) Synthesis and medical applications of oligosaccharides. *Nature* 446:1046–1051.
56. Singer SJ, Nicolson GL (1972) The fluid mosaic model of the structure of cell membranes. *Science* 175:720–731.
57. Lingwood D, Simons K (2010) Lipid rafts as a membrane-organizing principle. *Science* 327:46–50.
58. Sezgin E, Levental I, Mayor S, Eggeling C (2017) The mystery of membrane organization: Composition, regulation and roles of lipid rafts. *Nat Rev Mol Cell Biol* 18:361–374.
59. Heberle FA, et al. (2013) Bilayer thickness mismatch controls domain size in model membranes. *J Am Chem Soc* 135:6853–6859.
60. Nickels JD, et al. (2015) Mechanical properties of nanoscopic lipid domains. *J Am Chem Soc* 137:15772–15780.
61. Nickels JD, et al. (2017) The in vivo structure of biological membranes and evidence for lipid domains. *PLoS Biol* 15:e2002214.
62. Lehn J-M (2002) Toward self-organization and complex matter. *Science* 295:2400–2403.
63. Lehn J-M (2013) Perspectives in chemistry–Steps towards complex matter. *Angew Chem Int Ed Engl* 52:2836–2850.
64. Xiao Q, et al. (2016) Why do membranes of some unhealthy cells adopt a cubic architecture? *ACS Cent Sci* 2:943–953.
65. Zhang S, et al. (2014) Mimicking biological membranes with programmable glycan ligands self-assembled from amphiphilic Janus glycodendrimers. *Angew Chem Int Ed Engl* 53:10899–10903.
66. Zhang S, et al. (2015) Unraveling functional significance of natural variations of a human galectin by glycodendrimersomes with programmable glycan surface. *Proc Natl Acad Sci USA* 112:5585–5590.
67. Kopitz J, et al. (2017) Reaction of a programmable glycan presentation of glycodendrimersomes and cells with engineered human lectins to show the sugar functionality of the cell surface. *Angew Chem Int Ed Engl* 56:14677–14681.
68. Xiao Q, et al. (2018) Exploring functional pairing between surface glycoconjugates and human galectins using programmable glycodendrimersomes. *Proc Natl Acad Sci USA* 115:E2509–E2518.
69. Yeung SY, et al. (2017) Reversible self-assembled monolayers (rSAMs): Adaptable surfaces for enhanced multivalent interactions and ultrasensitive virus detection. *ACS Cent Sci* 3:1198–1207.
70. Schulz M, Binder WH (2015) Mixed hybrid lipid/polymer vesicles as a novel membrane platform. *Macromol Rapid Commun* 36:2031–2041.
71. Vatankhah-Varnosfaderani M, et al. (2018) Chameleon-like elastomers with molecularly encoded strain-adaptive stiffening and coloration. *Science* 359:1509–1513.
72. Damasceno PF, Engel M, Glotzer SC (2012) Predictive self-assembly of polyhedra into complex structures. *Science* 337:453–457.
73. Kaplan CN, et al. (2017) Controlled growth and form of precipitating microsculptures. *Science* 355:1395–1399.
74. Farokhzad OC, Langer R (2009) Impact of nanotechnology on drug delivery. *ACS Nano* 3:16–20.
75. Morandat S, Azouzi S, Beauvais E, Mastouri A, El Kirat K (2013) Atomic force microscopy of model lipid membranes. *Anal Bioanal Chem* 405:1445–1461.
76. Baumgart T, Hess ST, Webb WW (2003) Imaging coexisting fluid domains in biomembrane models coupling curvature and line tension. *Nature* 425:821–824.
77. Cebecauer M, et al. (2018) Membrane lipid nanodomains. *Chem Rev* 118:11259–11297.